Intuitive and Accurate Patient-Specific Coronary Tree Modeling from Cardiac Computed-Tomography Angiography

M. Wels[1], F. Lades[2], C. Hopfgartner[2], C. Schwemmer[1], and M. Suehling[1]

[1] Siemens Healthcare GmbH, Forchheim, Germany
[2] ISO-Gruppe, Nuremberg, Germany

Abstract. In cases of suspected coronary heart disease, diagnosis and subsequent, potentially interventional, treatment are heavily dependent on the status of a patient's coronaries and how their capabilities to ensure blood supply to the heart muscle are affected by the disease. This status may be comprehensively assessed by exact three-dimensional geometric models of the coronary arteries, which may then also serve as input for higher-level functional analysis like computational hemodynamics. While fully-automatic modeling approaches from non-invasive Cardiac Computed-Tomography Angiography data exist, these however lack absolute reliability, and manual editing of the initially detected geometric model is often required. Systems about to be accepted in clinical routine thus require intuitive and time efficient editing capabilities. We therefore present an interactive 3D modeling method which is embedded in an end-to-end coronary modeling system based on implicit surface interpolation from 3D surface constraints using compactly supported Radial Basis Functions. This approach is of excellently manageable computational complexity and allows providing a virtually real-time system for patient-specifically modeling coronary trees. Inconsistent user input is handled by tangent frame bundles allowing adequate dismissal of contradictory surface constraints. We have evaluated our 3D modeling method in a user study on 18 publicly available benchmark data sets from the Rotterdam Coronary Artery Algorithm Evaluation Framework with about 2,550 mm annotated ground-truth coronary lumen sections in total. Before editing, initial average mean surface distances were 0.61 mm and 0.69 mm for predefined healthy and diseased lumen sections of varying length. After $3'\ 38''$ of editing on average, achieved scores were 0.14 mm and 0.20 mm respectively. [1]

1 Introduction

Today's Cardiac Computed Tomography Angiography (CCTA) is able to provide detailed insight into patients' coronaries and their supply of blood to the heart. The rich morphological information contained in the data paves the way to

[1]The concepts and information presented in this article are based on research and are not commercially available. Patent pending (EP 16170187.5).

higher-level functional analysis of the depicted vessels, e.g. by computational hemodynamics, potentially replacing invasive procedures in a majority of cases. In order to be of use to this kind of analysis, a patient's coronaries need to be adequately geometrically modeled, i.e. the imaging data needs to be semantically enriched by patient-specific smooth three-dimensional surface data.

Clinical acceptance of fully-automatic approaches to do so is often hampered by non-intuitive and therefore time-consuming editing tools for subsequent exact and reproducible adjustment. In a clinical workstation set-up a smooth embedding of such a tool in the regular workflow is mandatory: only this allows the user to achieve his ultimate goal, which is having a patient-specific 3D model of a patient's coronaries meeting the accuracy needs imposed by the planned subsequent functional analysis in an acceptable amount of time.

We therefore present a novel solution for the associated problem of accurately and patient-specifically modeling the coronary tree from 3D CCTA data. Our solution is a two-step approach: after an initial fully automatic centerline detection [11] and vessel lumen segmentation [6] we offer interactive centerline and lumen editing not only on orthogonal cross-sectional views, but also on curved planar reformatted (CPR) views. This becomes possible by accepting user input on these views and by appropriately transferring it to 3D surface samples for implicit surface representation with Radial Basis Functions (RBFs). Contradictory user input is handled using tangent frame bundles for adequate surface sample dismissal. User interaction is designed in a way that is equally user-friendly, transparent, robust and flexible with regard to the finally achieved geometric models.

Our research is most related to the work of Kretschmer et al. [5] who address the same scenario. While our method relies on implicit 3D surface modeling via compactly supported RBFs, they use implicit surface sweeps. The latter, however, limits editing interaction to cross-sectional views while editing on CPR views is not covered. In CPR views, though, complete coronary arteries from the ostia to their distal ends including lumen segmentation (if available) can be quicker assessed and validated than in cross-sectional views. Furthermore, Kretschmer et al. [5] do not explicitly address surface sample consistency. With our novel technique even contradictory surface samples can be managed in 3D while being able to be edited also from non-linearly reformatted views like the CPRs, which—to the best of our knowledge—has not been dedicatedly addressed by any previous work so far. Other than that, our system follows the conceptual pipeline introduced in Reference [5] including blending and isosurface extraction.

The technique of modeling 3D surfaces via RBFs has been introduced by Savchenko et al. [8] and has been successfully applied and developed further by other researchers afterwards [9, 2]. Compactly supported RBFs for interpolating implicit surfaces as used in our method are discussed in Reference [7]. They are the key to making our approach suited for interactive real-time applications as realized in our software prototype.

While many scientific publications address individual components of our pipeline, our research is embedded in a complete end-to-end system from CCTA

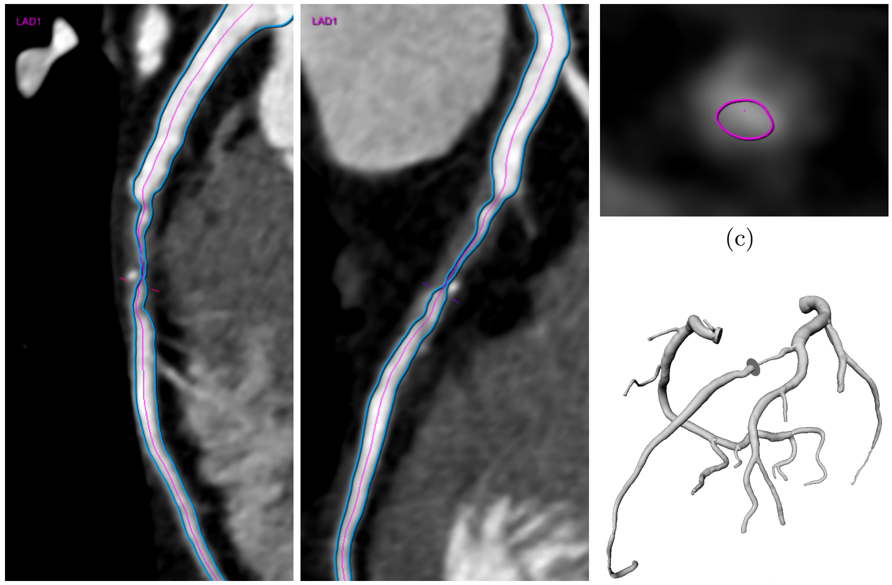

(a) (b) (c) (d)

Fig. 1. A patient's Left Anterior Descending (LAD) coronary artery in a 90° twin CPR view (a, b), a cross-sectional view (c), and a 3D rendering of the coronary tree after isosurface extraction from our implicit RBF-based surface representation (d).

data to the accurately and smoothly modeled lumen (see Fig. 1), including our novel intuitive and user-friendly capability of manual correction, ready for further usage, e.g. for volumetric measurements, stenosis grading, plaque characterization, or computational hemodynamics [3]. For all these relevant medical inquiries, our method makes clinical workstation solutions conceivable.

2 Methods

2.1 3D Surface Representation with Radial Basis Functions

Let $\mathcal{S} = \{\boldsymbol{p}_k = (p_k^x, p_k^y, p_k^z)^T \in \mathbb{R}^3 | k = 1, \ldots, N\}$ be a set of 3D surface samples consisting of 3D points that are lying on a vessel surface. In our system, individual surfaces of vessels from the ostia to their distal end are implicitly represented by RBFs of the form

$$f(\boldsymbol{p}) = \sum_{j=1}^{N'} c_j \phi(|\boldsymbol{p} - \boldsymbol{p}_j|) + q(\boldsymbol{p}) \tag{1}$$

where $\boldsymbol{p} \in \mathbb{R}^3$, $N' = 3N$, $|.|$ is the Euclidean norm, and ϕ is the basic function. The degree one polynomial q states the linear and constant portions of f. The function values are $f(\boldsymbol{p}) < 0$ for $\boldsymbol{p}$ inside the vessel, $f(\boldsymbol{p}) > 0$ outside the vessel, and $f(\boldsymbol{p}) = 0$ on the vessel surface itself. In order to turn functions of this kind into valid surface representations, the appropriate coefficients c_j need to be found from given constraints with known function value $h_i = f(\boldsymbol{p}_i)$. This yields

$$h_i = \sum_{j=1}^{N'} c_j \phi(|\boldsymbol{p}_i - \boldsymbol{p}_j|) + q(\boldsymbol{p}_i). \tag{2}$$

For each surface point $\boldsymbol{p}_k \in \mathcal{S}$ and associated normal vectors $\boldsymbol{n}_k$ and for some scalar value $\lambda \in \mathbb{R}$, these constraints can be defined by $h_i = f(\boldsymbol{p}_i) = 0$ for surface points $\boldsymbol{p}_i = \boldsymbol{p}_k$, $h_i = f(\boldsymbol{p}_i) < 0$ for offset points $\boldsymbol{p}_i = \boldsymbol{p}_k - \lambda \boldsymbol{n}_k$ inside and $h_i = f(\boldsymbol{p}_i)) > 0$ for $\boldsymbol{p}_i = \boldsymbol{p}_k + \lambda \boldsymbol{n}_k$ outside the 3D object. Where sample consistency in the sense of Carr et al. [2] cannot be guaranteed, offset points are omitted.

Equation (2) can be rewritten as the following system of linear equations

$$\begin{pmatrix} \boldsymbol{A} & \boldsymbol{P} \\ \boldsymbol{P}^T & \boldsymbol{0} \end{pmatrix} \begin{pmatrix} \boldsymbol{c} \\ \boldsymbol{q} \end{pmatrix} = \begin{pmatrix} \boldsymbol{h} \\ \boldsymbol{0} \end{pmatrix} \tag{3}$$

where $\boldsymbol{P} = ((1, p_1^x, p_1^y, p_1^z), \ldots, (1, p_{N'}^x, p_{N'}^y, p_{N'}^z))^T$ and $\boldsymbol{q} = (q_0, \ldots, q_3)^T$ and $\boldsymbol{A} = (\phi_{ij})_{i=1,\ldots,N', j=1,\ldots,N'}$ with $\phi_{ij} = \phi(|\boldsymbol{p}_i - \boldsymbol{p}_j|)$. This system is symmetric and positive semi-definite. In the case of basic functions with infinite support, e.g., biharmonic $\phi(x) = x$ or triharmonic $\phi(x) = x^3$ splines, $\boldsymbol{A}$ is dense and the system can be solved with direct solvers like symmetric LU decomposition or Cholesky decomposition. The involved computational complexity, however, restricts this approach to a comparably small number of surface samples limiting the modeling capabilities with respect to small details. Nonetheless small details are of particular interest when it comes to modeling the coronaries and to assessing the impact of calcified or non-calcified plaque in the intima on the remaining vessel lumen.

2.2 Compactly Supported Radial Basis Functions

In order to overcome this drawback of infinitely supported basic functions we have, in accordance with Morse et al. [7], chosen our basic function to be the compactly supported kernel $\phi(x) = (1 - x/\alpha)_+^2$ with support radius α, which is of C^0 continuity. This yields a sparse matrix $\boldsymbol{A}$ with most entries $\phi_{ij} = 0$ remote of the main diagonal. The parameter α is chosen according to the expected density of the surface samples. Additionally, a k-d tree is used to store and manage our surface samples according to the chosen radius of support. Both make our system computationally more efficient in building and in solving the associated system of linear equations and in evaluating the RBFs (Eqn. (1)), e.g. for visualizing real-time CPR overlays, yielding immediate system responses after surface sample updates by means of editing operations even in the case of hundreds of surface samples. For instance, building and solving a system formed from about 800 surface points using sparse Cholesky decomposition only takes roughly 50 ms on our hardware.

Initial surfaces are generated from fully automatic detection results [11, 6] by surface re-sampling and using the resulting points in the above sense for a primary RBF interpolation.

2.3 Tangent Frame Bundles for Surface Sample Consistency

Let $\boldsymbol{c}(t) \in \mathbb{R}^3$, $t \in [0,1]$, be a spline representing a vessel centerline. This spline can be used to compute so-called tangent frame bundles $\boldsymbol{T}(t) = (\boldsymbol{r}_1(t), \boldsymbol{r}_2(t), \boldsymbol{r}_3(t)) \in \mathcal{SO}(3)$, $t \in [0,1]$. While the rotations $\boldsymbol{T}(t)$ and $\boldsymbol{c}(t)$ can be used to create the well-known two-dimensional CPR visualization, the associated differential geometry can equivalently be used to map 2D input back to 3D in order to collect 3D surface samples defining altered courses of the initial 3D surface.

Managing of surface samples, and in particular dismissal of contradictory samples when editing surfaces on CPR views in this manner, is also realized by means of tangent frame bundles, which are initialized from the latest user input, transferred to world coordinates, and the centerline currently selected for curved planar visualization. For this we use special tangent frame bundles $\boldsymbol{T}^*(t)$ (see Fig. 2) where the first axis $\boldsymbol{r}_1^*(t)$ of each rotation orthogonally points in the direction of a spline defined by user-set control points, which are supposed to determine the new course of the vessel surface, and the second one, $\boldsymbol{r}_2^*(t)$, aligns with another spline's, i.e. the centerline's, tangents. Using the function $\boldsymbol{T}^*(t_i)$ for (in our case) approximated orthogonal projections t_i on the current centerline [5], which are associated with existing surface samples $\boldsymbol{p}_i$, it is possible to base decision for contradictory surface point dismissal on the relations $\arccos(\boldsymbol{T}^*(t_i)^{-1} \cdot (\boldsymbol{p}_i - \boldsymbol{c}_i) \bullet \boldsymbol{r}_1^*(t_i)) \leq \beta$, where β is an angle. Practical values of β are lying between 45° and 90°.

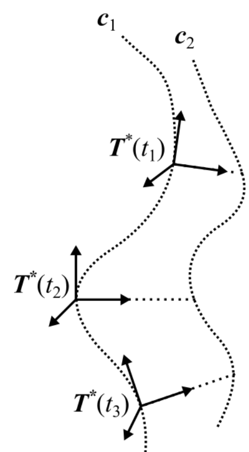

Fig. 2. Special tangent frame bundles derived from two splines.

For editing operations on cross-sectional views it is sufficient to base this decision on $|t_i - t^*| < \frac{\epsilon}{2}$ where ϵ is the normalized rejection area about a newly drawn contour at parameter t^* along the centerline $\boldsymbol{c}$.

2.4 Coronary Tree Blending and Isosurface Extraction

In order to model the whole coronary tree, individual implicit surface branches f_i (as in Eqn. (1)) must be unified to form a global implicit surface g. For having smooth joints at vessel bifurcations we blend our branches using the following field function similar to [5]:

$$f^w(\boldsymbol{p}) = \begin{cases} -1 & \text{if } f(\boldsymbol{p}) < -w, \\ \frac{f(\boldsymbol{p})}{2w} - 0.5 & \text{if } -w <= f(\boldsymbol{p}) <= w, \text{ and} \\ 0 & \text{if } w < f(\boldsymbol{p}). \end{cases} \tag{4}$$

This allows solid union using the min operator yielding

$$g(\boldsymbol{p}) = \min_i f_i^w(\boldsymbol{p}). \tag{5}$$

The parameter w defines the radius of support and can be set empirically. Now $g(\boldsymbol{p}) = -0.5$ is the coronary tree's isosurface.

For visualization purposes and for interactive sessions we use a propagation-based marching cubes algorithm [1] as suggested in Reference [5] that restricts evaluation of g to cells close to the isosurface. A typical result of this is depicted in Fig. 1 (d).

3 Experimental Setting and Results

We have evaluated our system, which has been implemented relying on MeVisLab 2.7 (64 Bit), on a regular workstation with Intel Xeon Processor W3536 (2×3.30 GHz) and 12 GB RAM.

In order to validate the major claim of our proposed solution, i.e. providing the clinical researcher or practitioner with means to fast and accurately model the coronaries' geometry at sub-voxel accuracy with maximum controllability even from non-linearly reformatted views like the CPR views, we carried out the following experiment: during manual geometric modeling with our development prototype software we visualized the available ground-truth annotations in the CPR views and in the cross-sectional views as colored 2D contour overlays. The experiment's task for the test person now was not modeling from the underlying medical image evidence but rather from the displayed ground-truth. This way a real-world scenario could be simulated, where the user has its own understanding of the actual course of the continuous true surfaces underlying the image evidence apart from any medical image formation insufficiencies (partial volume effects, blooming artifacts, limited spatial resolution, etc.). We used a subset of the training data collection from the Rotterdam Coronary Artery Algorithm Evaluation Framework [4], which consists of 18 patient data sets with automatically traced and manually corrected coronary centerlines [10] and 78 annotated coronary artery lumen sections, of which about 1,880 mm are classified as healthy and about 670 mm as diseased sections. The visualized ground-truth was chosen to be the annotations of "Observer 1". The respondent was asked to edit each lumen section starting from a tube structure which was curved but regular in diameter until he felt satisfied with the achieved result. The latter occurred after $3'\ 38''$ on average.

In terms of the Mean Surface Distance (MSD), where 0.06 mm and 0.08 mm would be the maximum achievable scores when exactly matching the ground-truth, the respondent reached an average score of 0.14 mm and 0.20 mm on the healthy and diseased lumen sections respectively. The average Maximum Surface Distances (Max. SD) per lumen section were 1.40 mm and 1.86 mm, where 2.25 mm and 2.61 mm are the values for the ground-truth annotations. The values immediately after initialization with a curved tube of regular diameter were 0.61 mm and 0.69 mm (MSD) and 1.64 mm and 2.09 mm (Max. SD) for healthy and diseased sections respectively. It must be noted that our final results are considerably closer to the ground-truth than results of any fully automatic method [4] and therefore emphasize the possible added value from manual surface correction using our method. Figure 3 gives reference of the development of accuracy during editing an individual diseased vessel section from our experiment over time.

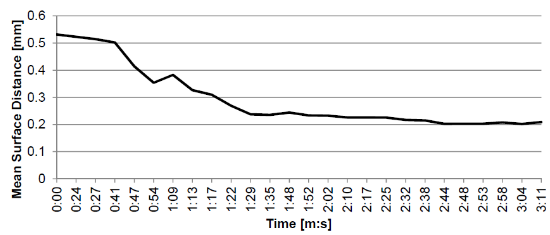

Fig. 3. The increase in modeling accuracy over time for a diseased vessel section (26.7 mm) from our experiment.

All values were computed using the Rotterdam Coronary Artery Algorithm Evaluation Framework's evaluation executable, where by design through discretizing effects even the ground-truth, which we converted from individual cross-sectional contours to surface meshes by applying the VTK Ruled Surface Filter, apparently may not achieve perfect segmentation scores. The remaining surface errors, whose magnitude is small enough not to be of practical clinical relevance, are due to discontinuities of the ground-truth annotations that cannot be represented with our smooth interpolator. Furthermore, we did not change the course of the loaded centerlines [10], which in our software prototype are not allowed to run outside the annotated vessel lumen. In rare cases, where this was true for the ground-truth annotations, associated lumen sections could necessarily not be modeled to the full satisfaction of our test person. Further errors can be explained by quantization errors when re-using the discrete CPR formation (512×512 pixels) in the reverse direction for mapping surface samples back to 3D in our software prototype.

4 Conclusions

We presented a quasi-real-time interactive method for modeling coronary arteries in 3D from CCTA data. It is embedded in an end-to-end processing pipeline starting from the 3D medical image volume to—over coronary tree tracing and fully-automatic vessel lumen segmentation—the final three-dimensional and manually correctable geometric models. As a core contribution our method allows fast geometric modeling and model adaptation using compactly supported RBFs. By managing surface constraints with tangent frame bundles, which is another major contribution of our work, surface sample consistency can be guaranteed even when editing in non-linearly reformatted views like the CPR views. Our experiments show that with our method automatically computed geometric models can be considerably improved, finally reaching accuracy scores needed for further higher-level analysis like hemodynamic simulations or similar.

References

1. C. L. Bajaj, V. Pascucci, and D. R. Schikore. Fast Isocontouring for Improved Interactivity. In *Proceedings of the 1996 Symposium on Volume Visualization*, VVS '96, pages 39–46, Oct. 1996.
2. J. C. Carr, R. K. Beatson, J. B. Cherrie, T. J. Mitchell, W. R. Fright, B. C. McCallum, and T. R. Evans. Reconstruction and Representation of 3D Objects with Radial Basis Functions. In *Proceedings of the 28th Annual Conference on Computer Graphics and Interactive Techniques*, SIGGRAPH '01, pages 67–76, Los Angeles, CA, USA, Aug. 2001.
3. L. Itu, P. Sharma, T. Passerini, A. Kamen, C. Suciu, and D. Comaniciu. A Parameter Estimation Framework for Patient-Specific Hemodynamic Computations. *Journal of Computational Physics*, 281:316–333, Jan. 2015.
4. H. Kirişli, M. Schaap, C. Metz, A. Dharampal, W. B. Meijboom, S. L. Papadopoulou, A. Dedic, K. Nieman, M. A. de Graaf, M. Meijs, M. Cramer, A. Broersen, S. Cetin, A. Eslami, L. Flórez-Valencia, K. L. Lor, B. Matuszewski, I. Melki, B. Mohr, I. Ösüz, R. Shahzad, C. Wang, P. Kitslaar, G. Unal, A. Katouzian, M. Orkisz, C.-M. Chen, F. Precioso, L. Najman, S. Masood, D. nay, L. van Vliet, R. Moreno, R. Goldenberg, E. Vuçini, G. Krestin, W. Niessen, and T. van Walsum. Standardized Evaluation Framework for Evaluating Coronary Artery Stenosis Detection, Stenosis Quantification and Lumen Segmentation Algorithms in Computed Tomography Angiography. *Medical Image Analysis*, 17(8):1–18, Dec. 2013.
5. J. Kretschmer, C. Godenschwager, B. Preim, and M. Stamminger. Interactive Patient-Specific Vascular Modeling with Sweep Surfaces. *IEEE Transactions on Visualization and Computer Graphics*, 19(12):2828–2837, Dec. 2013.
6. F. Lugauer, Y. Zheng, J. Hornegger, and B. M. Kelm. Precise Lumen Segmentation in Coronary Computed Tomography Angiography. In *Medical Computer Vision: Algorithms for Big Data*, MCV '14, pages 137–147, Cambridge, MA, USA, Sept. 2014.
7. B. S. Morse, T. S. Yoo, P. Rheingans, D. T. Chen, and K. R. Subramanian. Interpolating Implicit Surfaces from Scattered Surface Data Using Compactly Supported Radial Basis Functions. In *International Conference on Shape Modeling and Applications*, SMI '01, pages 89–98, May 2001.
8. V. V. Savchenko, A. A. Pasko, O. G. Okunev, and T. L. Kunii. Function Representation of Solids Reconstructed from Scattered Surface Points and Contours. *Computer Graphics Forum*, 14(4):181–188, 1995.
9. G. Turk and J. F. O'Brien. Shape Transformation Using Variational Implicit Functions. In *Proceedings of the 26th Annual Conference on Computer Graphics and Interactive Techniques*, SIGGRAPH '99, pages 335–342, New York, NY, USA, 1999.
10. G. Yang, A. Broersen, R. Petr, P. Kitslaar, M. A. de Graaf, J. J. Bax, J. Reiber, and J. Dijkstra. Automatic Coronary Artery Tree Labeling in Coronary Computed Tomographic Angiography Datasets. In *Computing in Cardiology*, CinC '11, pages 109–112, Hangzhou, China, Sept. 2011.
11. Y. Zheng, H. Tek, and G. Funka-Lea. Robust and Accurate Coronary Artery Centerline Extraction in CTA by Combining Model-Driven and Data-Driven Approaches. In *International Conference on Medical Image Computing and Computer-Assisted Intervention, Nagoya, Japan*, MICCAI '13, pages 74–81, Sept. 2013.